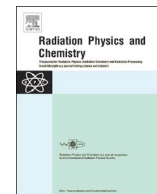




Contents lists available at ScienceDirect

## Radiation Physics and Chemistry

journal homepage: [www.elsevier.com/locate/radphyschem](http://www.elsevier.com/locate/radphyschem)

## Dosimetry assessment of DNA damage by Auger-emitting radionuclides: Experimental and Monte Carlo studies

S. Di Maria<sup>a,\*</sup>, A. Belchior<sup>a</sup>, E. Pereira<sup>a</sup>, L. Quental<sup>a</sup>, M.C. Oliveira<sup>a</sup>, F. Mendes<sup>a</sup>, J. Lavrado<sup>b</sup>, A. Paulo<sup>a</sup>, P. Vaz<sup>a</sup>

<sup>a</sup> Centro de Ciências e Tecnologias Nucleares, Instituto Superior Técnico, Universidade de Lisboa, Estrada Nacional 10, km 139,7, 2695-066 Bobadela LRS, Portugal

<sup>b</sup> iMed.UlIsboa, Faculdade de Farmácia, Universidade de Lisboa, Av. Prof. Gama Pinto, 1649-003 Lisboa, Portugal

## ARTICLE INFO

## Keywords:

Nano dosimetry  
Auger emitter radionuclides  
Monte Carlo simulations  
DNA damage

## ABSTRACT

Recently there has been considerable effort to investigate the potential use and efficacy of Auger-electron emitters in targeted radiotherapy. Auger electrons travel a short distance within human tissues (at nano-scale level) and, therefore, if an Auger-emitting radionuclide is transported to the cell nucleus it will cause enhanced DNA damage. Among the Auger-emitting radionuclides,  $^{125}\text{I}$  is of particular interest, as it emits about 25 electrons per decay.  $^{99\text{m}}\text{Tc}$  only emits 5 electrons per decay, but presents some attractive characteristics such as a short half-life, easy procurement and availability and ideal imaging properties for therapy monitoring.

In order to study the dosimetric behavior of these two radionuclides ( $^{125}\text{I}$  and  $^{99\text{m}}\text{Tc}$ ) at nano-scale sizes and given the DNA-intercalation properties of Acridine Orange (AO), we have designed  $^{99\text{m}}\text{Tc}$  (I)-tricarbonyl complexes and  $^{125}\text{I}$ -heteroaromatic compounds that contain AO derivatives, in order to promote a closer proximity between the radionuclides and the DNA structure. With the aim to have an insight on the relevance of these radiolabelled compounds for DNA-targeted Auger therapy, different aspects were investigated: i) their ability to cause DNA strand breaks; ii) the influence of the two different radionuclides in DNA damage; iii) the effect of the distance between the AO intercalating unit and the radioactive atom ( $^{99\text{m}}\text{Tc}$  or  $^{125}\text{I}$ ). To address these issues several studies were carried out encompassing the evaluation of plasmid DNA damage, molecular docking and nanodosimetric Monte Carlo modelling and calculations. Results show that the two classes of compounds are able to induce DNA double strand breaks (dsb), but the number of DNA damages (e.g. dsb yield) is strongly dependent on the linker used to attach the Auger emitting radionuclide ( $^{125}\text{I}$  or  $^{99\text{m}}\text{Tc}$ ) to the AO moiety. In addition, nanodosimetric calculations confirm a strong gradient of the absorbed energy with the DNA-radionuclide distance for the two radionuclides studied. Finally these results show the existence of a critical distance (of about 11 Å) beyond which it is probable that the direct effects start to be ineffective in DNA damage induction.

### 1. Introduction

Molecular radiotherapy is an anticancer technique based on the use of radiopharmaceuticals, which are drugs containing radionuclides emitting ionizing radiation ( $\beta$  and  $\alpha$  particles or Auger-electrons). Many of these radionuclides are also gamma- or positron-emitters and for this reason are also useful for imaging applications, such as single-photon emission computerized tomography (SPECT) or positron emission tomography (PET) imaging. The possible simultaneous use of these two main capabilities (radiotherapy and imaging) makes these types of radionuclides very attractive from the theranostic point of view (Falzone et al., 2015). From the radiotherapy side, the Auger-electron emitters are considered potentially very promising because of their

extremely short range in biological tissues depositing their energy in very small volumes at the nanoscopic scale (of the order of DNA and nucleus dimensions) (Howell, 2008). Their use could be very specific and with a high local efficiency in tumor cells killing, leaving, in this way, the surrounding healthy tissue exempt from avoidable therapy damages. Among other radionuclides,  $^{125}\text{I}$  was widely studied for its eventual use in Auger-electron based cancer therapy (Howell, 2008).  $^{99\text{m}}\text{Tc}$  is the most used radionuclide for SPECT imaging in diagnostic nuclear medicine; however, in recent years,  $^{99\text{m}}\text{Tc}$  has also been investigated for its potential use in Auger cancer therapy (Esteves et al., 2010). This increasing interest is due to some particular  $^{99\text{m}}\text{Tc}$  characteristics (such as short half-life and availability) that are very favorable for its clinical use. However, to foster their use as therapeutic

\* Corresponding author.

<http://dx.doi.org/10.1016/j.radphyschem.2017.01.028>

Received 16 September 2016; Received in revised form 17 January 2017; Accepted 25 January 2017  
0969-806X/ © 2017 Elsevier Ltd. All rights reserved.

Auger emitters, further studies and deeper investigation of the biological effects and dosimetry inherent to both radionuclides ( $^{125}\text{I}$  and  $^{99\text{m}}\text{Tc}$ ) are necessary, from several points of view.

The main objective of this work is to study how the distance of the radionuclide ( $^{125}\text{I}$  and  $^{99\text{m}}\text{Tc}$ ) from the target-DNA influences the DNA lesion efficiency in terms of quantities such as the double strand break (DSB) yield and absorbed energy in DNA volumes. As explained in the next sections, to reach this goal, experimental studies (plasmid experiments) were undertaken, complemented by state of the art Monte Carlo (MC) simulation tools to perform nanodosimetry modelling and calculations.

## 2. Materials and methods

### 2.1. Plasmid experiments

The in vitro assessment of the DNA damage induced by an Auger-emitting radionuclide can be performed by exposing a model circular plasmid DNA to the desired chemical form of the radionuclide. The presence and relative abundance of each conformation (supercoiled (SC), open circular (OC) and linear (Lin)) of the plasmid can be easily assessed by gel electrophoresis. A single strand break (SSB) transforms supercoiled DNA into open circular, whereas a double strand break (DSB) transforms supercoiled DNA into linear DNA. In this study only DSBs were taken into account.

Moreover, the role of direct versus indirect effects on the DNA damage can be estimated by performing the plasmid irradiation in the presence of radical scavengers, like dimethyl sulfoxide DMSO. The scavengers react with the reactive oxygen species (ROS) and avoid the DNA damage due to indirect effects (Balagurumoorthy et al., 2006). The ability of the radioiodinated derivatives ( $^{125}\text{I-C}_3$ ,  $^{125}\text{I-C}_5$  and  $^{125}\text{I-C}_8$ ) and  $^{99\text{m}}\text{Tc}$  complexes ( $^{99\text{m}}\text{Tc-C}_3$  and  $^{99\text{m}}\text{Tc-C}_5$ ) to induce DNA damage was studied by incubating the different radio-compounds with supercoiled  $\phi\text{X174}$  plasmid DNA at 4 °C. In Table 1, the different distances between radionuclides and DNA helical axis as estimated by molecular docking simulations (Molecular Operating Environment, 2013) are shown.

For a reliable comparison of the efficacy of each compound to induce DNA damage, the plasmids were exposed to a similar number of increasing accumulated decays. Given the differences in the  $^{99\text{m}}\text{Tc}$  and  $^{125}\text{I}$  half-lives, two approaches were used:

- $^{99\text{m}}\text{Tc}$  ( $T_{1/2}=6.02$  h): the same concentration of  $\phi\text{X174}$  plasmid was exposed for 24 h to increasing amounts of each complex, in independent samples, with applied activities spanning between 5 and 500  $\mu\text{Ci}$ . At the end of incubation, each reaction mixture was analyzed by gel electrophoresis to separate the different DNA isoforms that were quantified by densitometry.
- $^{125}\text{I}$  ( $T_{1/2}=60.4$  days):  $\phi\text{X174}$  plasmid DNA was exposed to a fixed initial amount (about 40  $\mu\text{Ci}$ ) of each  $^{125}\text{I}$ -labeled molecule up to 28 days, and aliquots of the reaction mixture were analyzed every 7 days by gel electrophoresis.

**Table 1**

Distance between the radionuclide in the intercalated AO derivatives and the DNA helical axis obtained by molecular modelling simulations.

Linker	Distance to DNA axis (Å)	
	$^{125}\text{I}$	$^{99\text{m}}\text{Tc}$
C <sub>3</sub>	9.37	10.80
C <sub>5</sub>	10.49	12.92
C <sub>8</sub>	11.04	–

### 2.2. Monte Carlo simulations

Electrons fluxes and deposited energies were calculated through the state-of-art MC simulation program MCNP6 (MCNP6, 2013). Considering the electron transport, the ENDF/B VI.8 database contains cross sections for atomic excitation, electron elastic scattering, subshell electro-ionization and bremsstrahlung and is able to simulate electron energies down to 10 eV (Hughes, 2014). An important development in the MCNP6 MC Code version was the introduction of a single-event electron transport for energies below 1 keV, a completely different approach used for higher energies with the condensed-history method (Hughes, 2014), making it a more suitable MC code for nanodosimetric calculations. MC simulations were used to calculate the absorbed energies in nanometric DNA volumes, and the results were qualitatively compared (assuming that for a given radiation quality the local energy deposition could be proportional to the ionization cluster size) with DSBs plasmid DNA experiments performed for this study. In this type of simulations only the physical stage (space distribution of ionization excitations and elastic scattering between the first  $10^{-15}$  s and  $10^{-13}$  s of interaction) was taken into account. Pre-chemical and chemical stages (diffusion and interaction of water radicals and molecular products) are not considered (Nikjoo et al., 2006), and for this reason the indirect effects on DSBs were not estimated through MC simulations.

### 2.3. Geometrical setup for MC simulations

Deposited energies were calculated in a volume corresponding to the DNA segment of 10 base pairs length and a nucleosome, both modeled as liquid water cylinders with nanometric dimensions (Lazakaris et al., 2012). Liquid water is the main constituent of the human body and represents a good approximation for soft biological tissue (Dingfelder et al., 2008).

Fig. 1 illustrates the geometrical setup of the MC simulations performed with the MCNP6 code. The DNA segment was modeled as a water cylinder of 2.3 nm diameter and 3.4 nm heights. This cylinder was set inside another water cylinder with 6 nm diameter and 10 nm height, which is equivalent to the size of a nucleosome.

The axes of the DNA segment and nucleosome were aligned along the z-axis (height of the DNA cylinder, as shown in Fig. 1).

The electron Auger source was simulated as an isotropic source at different distances to the DNA center (see Fig. 1), both for the  $^{125}\text{I}$  and  $^{99\text{m}}\text{Tc}$  Auger, Coster-Kronig and super Coster-Kronig energy spectra (Kareziakes et al., 1992). For each MC simulation  $10^5$  particles were simulated. This value was chosen being a compromise between the computational time and the statistical uncertainties obtained (between about 1% and 3%).

## 3. Results and discussions

### 3.1. Experimental DSBs and MC DNA energy deposition comparison

Firstly, In order to test the accuracy of the MC results obtained in this work, a preliminary simulation setup was considered and the results were compared with existing MC data in the available literature. We would like to stress here that the accuracy in this context should be intended in relative and not in absolute terms. Namely, given the same setup, we tested if our MC results were in agreement with values obtained with other existing MC data. In particular the deposited energy in a water sphere of 2 nm radius due to a  $^{125}\text{I}$  Auger electron point source placed at its center was calculated. The result shows that the deposited energy for one  $^{125}\text{I}$  decay in the volume sphere is of the order of 800 eV. Considering the volume involved, this value would imply a deposited energy per mass unit of about 4 MGy, being this value in the range limits showed by Sastry et al. (1984) and Kassiss et al. (1987), where a value of about  $10^4$ – $10^7$  Gy is reported for a

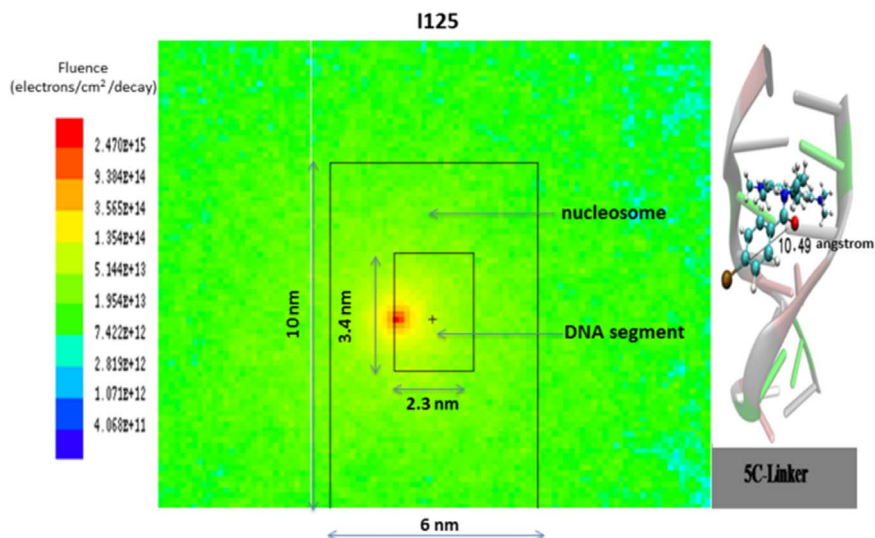


**Fig. 1.** Geometry setup used for MCNP6 MC Simulations. The  $^{125}\text{I}$  isotropic source in this example configuration is placed at 10.49 Angstrom from the DNA segment center. Mesh tally values around the decay source represent the intensity of electron fluence.

similar geometry setup. Considering the energy and materials involved in these types of simulations, an absolute accuracy is very difficult to obtain given the lack of experimental data that take to high uncertainty values (Palmans et al., 2015; Uehara et al., 1999).

Fig. 2 shows the deposited energy in the DNA segment volume (according to the geometry setup described in Section 2.3), considering both  $^{125}\text{I}$  and  $^{99\text{m}}\text{Tc}$  radionuclides. MC results are normalized to the number of Auger electrons emitted by  $^{125}\text{I}$  and  $^{99\text{m}}\text{Tc}$  (25 and 5 respectively). The green shaded zone in the graph of Fig. 2 represents the distance range found by molecular modelling for the compounds tested experimentally (see Table 1).

For a quantitative view on the DNA damage induced by each compound, the number of DSBs per plasmid molecule was calculated as a function of the accumulated decays/mL. These data were used to obtain the DSB yields per decay that are presented in Table 2, together with the different compound-central DNA axis distances.

The relative uncertainties for the DSBs data of Table 2 are in the range of about 2–80%. The highest uncertainties observed for  $^{125}\text{I}$ -C8 and  $^{99\text{m}}\text{Tc}$ -C5 in the presence of DMSO reflect the poor statistics associated to the rather low number of DSBs that were induced by the compounds, under these conditions.

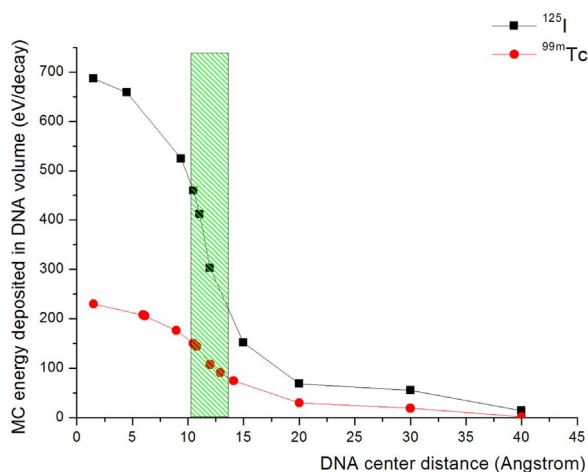


**Fig. 2.** Deposited energy in the DNA volume, obtained by MC simulations, with the decay sources ( $^{125}\text{I}$  and  $^{99\text{m}}\text{Tc}$ ) at different distances from the DNA center. The green shaded area represents the distance range found by molecular modelling for the compounds tested in the experimental studies. (For interpretation of the references to color in this figure legend, the reader is referred to the web version of this article.).

**Table 2**

Experimental DSB yield (Y) per decay obtained with plasmid experiments for  $^{99\text{m}}\text{Tc}$  and  $^{125}\text{I}$  compounds.

Compound/Distance to DNA	Y (DSB) ( $10^{-2}$ ) without DMSO	Y (DSB) ( $10^{-2}$ ) with DMSO
$^{125}\text{I}$ -C3 (9.37 Å)	$7.30 \pm 0.65$	$7.90 \pm 1.42$
$^{125}\text{I}$ -C5 (10.49 Å)	$4.80 \pm 0.14$	$3.70 \pm 0.07$
$^{125}\text{I}$ -C8 (11.04 Å)	$3.30 \pm 0.39$	$0.10 \pm 0.08$
$^{99\text{m}}\text{Tc}$ -C3 (10.49 Å)	$3.36 \pm 0.50$	$2.24 \pm 0.20$
$^{99\text{m}}\text{Tc}$ -C5 (12.92 Å)	$0.34 \pm 0.06$	$0.22 \pm 0.01$

Given the DSBs experimental  $^{125}\text{I}$  results, is quite evident that at a distance of 11.04 Angstrom the DSBs are mainly generated by indirect effects and most probably the critical distance in this case could be in the spatial range of 10.49–11.04 Angstrom. This value of critical distance for the  $^{125}\text{I}$  radionuclide is quite in agreement with the value indicated in the work of Balagurumorthy et al. (2012), where they indicate that at a distance greater than 12 Angstrom DSBs are exclusively produced by indirect effects. In the case of  $^{99\text{m}}\text{Tc}$ -C3, the DSB yield is of the same order of magnitude of the yields found for  $^{125}\text{I}$ . On the other hand,  $^{99\text{m}}\text{Tc}$  C5 presents a DSB yield that is one order of magnitude smaller than the  $^{125}\text{I}$  ones. Also, in this case there is no a clear trend indicating that a critical distance is present for  $^{99\text{m}}\text{Tc}$  where the direct effect start to be less effective (in the range of the distances studied).

From Fig. 3, a trend of smaller DSB yield and smaller DNA deposited energy values can be observed when the mean distance to DNA increases. Moreover, looking at the qualitative comparison between experimental DSB and MC deposited energy results (displayed in Fig. 3), it is easy to note that the theoretical results seem to overestimate the experimental DSBs at the longest distances to DNA. This trend was also previously observed by other authors for  $^{125}\text{I}$ -labeled DNA groove binders (Balagurumorthy et al., 2012). As invoked elsewhere (Balagurumorthy et al., 2012, 2008), these discrepancies can probably result from the use of a rigid rod like model for DNA in the MC calculations, while the supercoiled  $\phi\text{X174}$  plasmid DNA used to assess experimentally the DSB yield has a more flexible and dynamic structure.

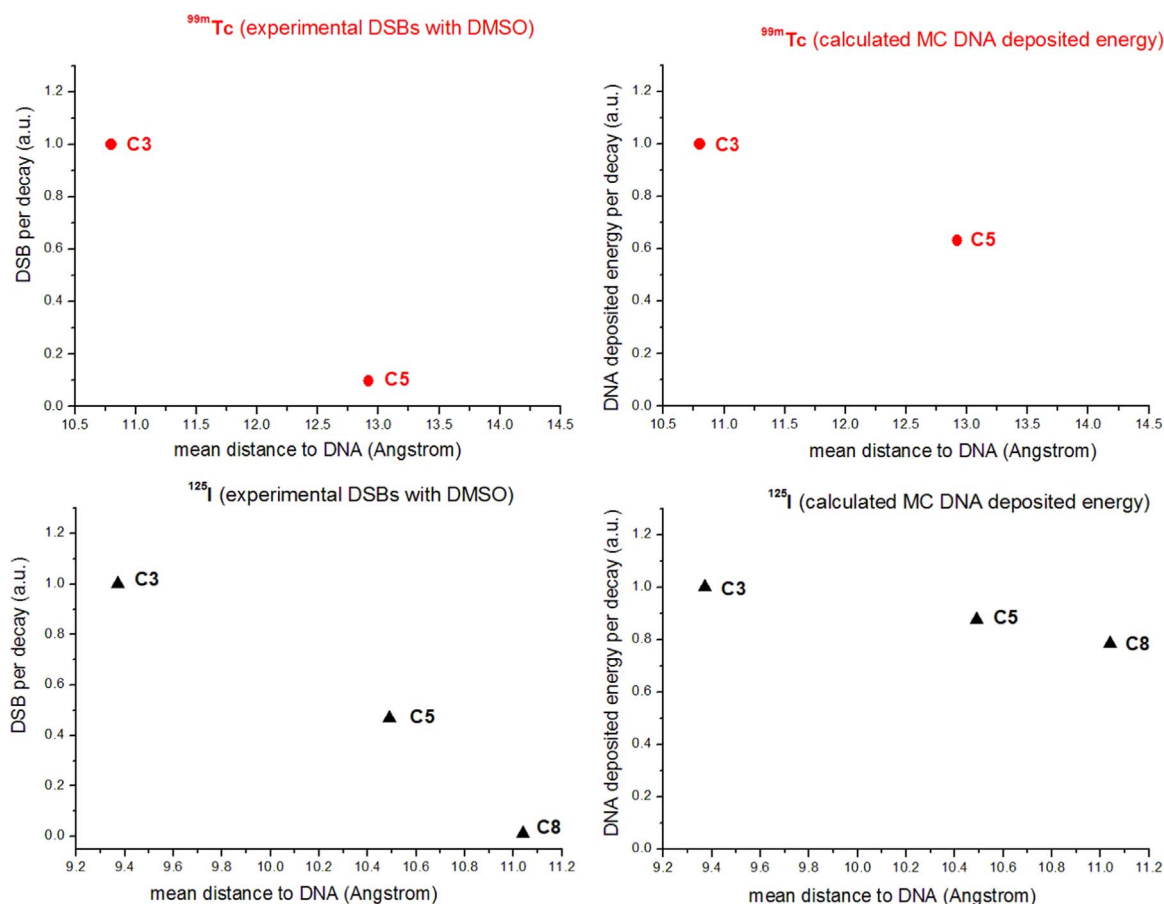


**Fig. 3.** Experimental DSB yield and calculated deposited energies for the different  $^{125}\text{I}$ -labeled derivatives and  $^{99m}\text{Tc}$  (I) complexes due only to direct effect. All the values reported (DSBs and deposited energies) are normalized to their maximum values.

### 3.2. MC Auger energy spectrum study

Considering the experimental results of Table 2, where a critical distance was not clearly assigned for the  $^{99m}\text{Tc}$  compounds, we investigated, through MC simulations, how the energy spectra characteristic of the  $^{125}\text{I}$  and  $^{99m}\text{Tc}$  Auger emitters could influence the energy deposition in the DNA segment. In order to accomplish this goal, as shown in the Table 3, the DNA deposited energy values were calculated per electron emitted (and not per decay) and for two general radionuclide-DNA axis distances (10.80 Å and 12.92 Å). Moreover the deposited energy obtained by using the Auger spectra source were also compared with the ones obtained using the mean energies of the two Auger spectra. As reported in Table 3, the DNA deposited energy for  $^{99m}\text{Tc}$  spectrum is always greater than the one obtained using the  $^{125}\text{I}$  spectrum (see columns 3 and 5 of Table 3). However, considering the

**Table 3**

Deposited energy in the DNA volume segment at a distance of 10.80 Å and 12.92 Å from the DNA center. The calculations were performed for  $^{99m}\text{Tc}$  and  $^{125}\text{I}$  Auger spectra and their respective mean energies.

Distance of source to center DNA axis (Å)	Deposited energy in DNA segment (eV/electron)			
	$^{99m}\text{Tc}$ Auger spectrum mean energy (224 eV)	$^{99m}\text{Tc}$ Auger Spectrum	$^{125}\text{I}$ Auger spectrum mean energy (575 eV)	$^{125}\text{I}$ Auger spectrum
10.80	43.26	22.80	17.21	15.60
12.92	32.14	18.27	10.33	11.12

two monochromatic energies of 224 eV and 575 eV (average energies of  $^{99m}\text{Tc}$  and  $^{125}\text{I}$  spectra respectively) the maximum deposition of energy in DNA segment for the two distances considered, is obtained with the monochromatic energy of 224 eV (see columns 2 and 4 of Table 3). These results are quite in agreement with other studies present in literature, where the maximum deposition of energy is around 200 eV for a DNA segment model similar to the one used in this study (Ftáčniková et al., 2000).

## 4. Conclusions

The experimental results obtained for  $^{125}\text{I}$  confirm the existence of a critical distance (between about 10.5 Å and 11 Å) beyond which the effectiveness of direct effects to produce DSB DNA lesions is substantially reduced. The MC results of the deposited energy study also show a strong gradient in the radionuclide-DNA center distances considered and have a tendency to overestimate the experimental results. In the experimental results for  $^{99m}\text{Tc}$  there is no direct evidence of the existence of a critical distance (passage from direct to indirect effects), at least at the range of distances calculated for the compounds tested. Also, given the energy spectrum characteristic of the Auger emitter  $^{99m}\text{Tc}$ , this radionuclide is able to generate higher energy deposition when the number of emitted electrons in  $^{99m}\text{Tc}$  and  $^{125}\text{I}$  is the same. The DSB efficiency can be considered, among many other issues, as a compromise between the spectral characteristic of the radionuclide Auger spectrum and the distance of the emitting source from the DNA center. Consequently, considering a fixed radionuclide-DNA axis distance, and given the spectral characteristic of  $^{99m}\text{Tc}$ , the radiation released by the decay of this radionuclide seems to be able to deposit a comparable energy (and probably to generate the same number of

DSBs) with respect to  $^{125}\text{I}$ , as can be seen for example in the  $^{125}\text{I}$ -C8 and  $^{99\text{m}}\text{Tc}$ -C3 configurations without DMSO (see Table 2).

Last but not least, sizable uncertainties affect both the MC (arising among other factors, from scarce, incomplete and non-existing cross-section data for very low electron energy for liquid water, with uncertainties values greater than 50% for energies less than 100 eV) (Sastry et al., 1984; Thomson et al., 2011) and the experimental results (related to the assessment of the radionuclide-DNA center distances, low statistics, etc.), and for this reason further studies will be necessary to further corroborate the obtained results.

## Acknowledgements

This work was supported by Fundação para a Ciência e Tecnologia (projects PTDC/QUI-QUI/114139/2009, EXCL/QEQ-MED/0233/2012, ID/Multi/04349/2013; and FCT Investigator to F. Mendes).

## References

- Balagurumoorthy, P., et al., 2012. Effect of distance between decaying  $^{125}\text{I}$  and DNA on Auger electron induced double-strand break yield. *Int J. Radiat. Biol.* 88 (12), 998–1008.
- Balagurumoorthy, P., Chen, K., Adelstein, S.J., Kassis, A.I., 2008a. Auger electron-induced double-strand breaks depend on DNA topology. *Radiat. Res.* 170, 70–82, (PubMed: 18582152).
- Balagurumoorthy, P., Chena, K., Bash, R.C., Adelstein, S.J., Kassis, A.I., 2006. Mechanisms underlying production of double-strand breaks in plasmid DNA after decay of  $^{125}\text{I}$ -hoechst. *Radiat. Res.* 166, 333–344.
- Dingfelder, M., et al., 2008. Comparisons of calculations with PARTRAC and NOREC: transport of electrons in liquid water. *Radiat. Res.* 169, 584–594.
- Esteves, T., Xavier, C., Gama, S., Mendes, F., Raposinho, P.D., Marques, F., Paulo, A., Pessoa, J.C., Rino, J., Viola, G., Santos, I., 2010. Tricarbonyl M(I) (M=Re,  $^{99\text{m}}\text{Tc}$ ) complexes bearing acridine fluorophores: synthesis, characterization, DNA interaction studies and nuclear targeting. *Org. Biomol. Chem.* 8, 4104–4116.
- Falzone, N., Fernández-Varea, J.M., Flux, G., Vallis, K.A., 2015. Monte Carlo evaluation of Auger electron-emitting theranostic radionuclides. *J. Nucl. Med.* 56, 1441–1446.
- Ftačnikova, S., Bohm, R., 2000. Monte Carlo calculations of energy deposition in dna for Auger emitters. *Radiat. Prot. Dosim.* 92 (4), 269–278.
- Howell, R., 2008. Auger processes in the 21st century. *Int J. Radiat. Biol.* 84 (12), 959–975.
- Hughes, G., 2014. Recent developments in low-energy electron/photon transport for MCNP6. *Prog. Nucl. Sci. Technol.* 4, 454–458.
- Kareziakes, J.G., Rao, D.V., Sastry, K.S.R., Howell, R.W., 1992. AAPM report N.37 (report of the task group N.6). *Med. Phys.* 19 (6).
- Kassis, A.I., Sastry, K.S., Adelstein, S.J., 1987b. Kinetics of uptake, retention, and radiotoxicity of  $^{125}\text{I}$ UDR in mammalian cells: implications of localized energy deposition by Auger processes. *Radiat. Res.* 109, 78–89, (PubMed: 3809393).
- Lazakaris, P., et al., 2012. Comparison of nanodosimetric parameters of track structure calculated by the Monte Carlo codes Geant4-DNA and PTRA. *Phys. Med. Biol.* 57, 1231–1250.
- MCNP6, 2013. initial release overview MCNP6 version 1.0, Los Alamos National Laboratory report LA-UR-13-22934
- Molecular Operating Environment (MOE), v.2013.08 software package 2013.08 edn ed. Montreal, Canada: Chemical Computing Group Inc
- Nikjoo, H., et al., 2006. Track-structure codes in radiation research. *Radiat. Meas.* 41, 1052–1074.
- Palmans, H., Rabus, H., Belchior, A.L., Bug, M.U., Galer, S., Giesen, U., et al., 2015. Future development of biologically relevant dosimetry. *Br. J. Radio.* 88, 20140392.
- Sastry, K.S.R., Rao, D.V., 1984. Dosimetry of low energy electrons. In: Rao, D.V., Chandra, R., Graham, M.C. (Eds.), *Physics of Nuclear Medicine: Recent Advances..* American Institute of Physics, Woodbury, NY, 169–208.
- Thomson, R.M., Kawrakow, I., 2011. On the Monte Carlo simulation of electron transport in the sub-1 keV energy range. *Med. Phys.* 38, 4531. <http://dx.doi.org/10.1118/1.3608904>.
- Uehara, S., et al., 1999. Comparison and assessment of electron cross sections for Monte Carlo track structure codes. *Radiat. Res.* 152, 202–213.